Probing the Specificity Determinants of Amino Acid Recognition by Arginase[†,‡]

Ekaterina Y. Shishova,[§] Luigi Di Costanzo,[§] Francis A. Emig,[||,⊥] David E. Ash,[*,||] and David W. Christianson[*,§]

Roy and Diana Vagelos Laboratories, Department of Chemistry, University of Pennsylvania, Philadelphia, Pennsylvania 19104-6323, and Department of Chemistry, Central Michigan University, Mount Pleasant, Michigan 48859

Received October 10, 2008; Revised Manuscript Received November 17, 2008

ABSTRACT: Arginase is a binuclear manganese metalloenzyme that serves as a therapeutic target for the treatment of asthma, erectile dysfunction, and atherosclerosis. In order to better understand the molecular basis of inhibitor affinity, we have employed site-directed mutagenesis, enzyme kinetics, and X-ray crystallography to probe the molecular recognition of the amino acid moiety (i.e., the α-amino and α-carboxylate groups) of substrate L-arginine and inhibitors in the active site of arginase I. Specifically, we focus on (1) a water-mediated hydrogen bond between the substrate α-carboxylate and T135, (2) a direct hydrogen bond between the substrate α-carboxylate and N130, and (3) a direct charged hydrogen bond between the substrate α-amino group and D183. Amino acid substitutions for T135, N130, and D183 generally compromise substrate affinity as reflected by increased K_M values but have less pronounced effects on catalytic function as reflected by minimal variations of k_{cat}. As with substrate K_M values, inhibitor K_d values increase for binding to enzyme mutants and suggest that the relative contribution of intermolecular interactions to amino acid affinity in the arginase active site is water-mediated hydrogen bond < direct hydrogen bond < direct charged hydrogen bond. Structural comparisons of arginase with the related binuclear manganese metalloenzymes agmatinase and proclavaminic acid amidinohydrolase suggest that the evolution of substrate recognition in the arginase fold occurs by mutation of residues contained in specificity loops flanking the mouth of the active site (especially loops 4 and 5), thereby allowing diverse guanidinium substrates to be accommodated for catalysis.

Arginase is a 105 kDa trimeric manganese metalloenzyme that catalyzes the hydrolysis of L-arginine to form L-ornithine and urea through a metal-activated hydroxide mechanism (*1*−*4*):

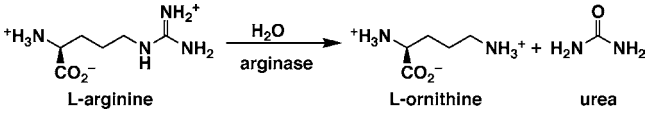

The hydrolysis of L-arginine is the final cytosolic step of the urea cycle in mammalian liver, and the activity of isozyme I is especially abundant in this organ (*5*−*7*). However, arginases I and II are also found in nonhepatic tissues, where these isozymes serve to regulate cellular levels of substrate L-arginine for nitric oxide biosynthesis (*8*−*10*) or cellular levels of product L-ornithine for polyamine biosynthesis via the generation of putrescine (*11*) or collagen biosynthesis via the generation of L-proline (*12*). Accordingly, arginase is a potential drug target for diseases in which L-arginine homeostasis and L-arginine-dependent biosynthetic pathways are disrupted due to aberrant upregulation of either one or both arginase isozymes, such as erectile dysfunction (*13*−*17*), asthma (*18*−*21*), or atherosclerosis (*22*−*25*).

L-Arginine is the sole biological substrate of arginase, and structural or stereochemical modifications of the amino acid substrate significantly attenuate binding and catalysis: D-arginine is not a substrate, and derivatization or deletion of the α-amino or α-carboxylate group of L-arginine yields alternative substrates with severely compromised kinetic properties (*26*). For example, substitution of the α-amino group with an α-hydroxyl group yields L-argininic acid, which exhibits a 9-fold increased K_M value and 3200-fold diminished catalytic activity based on k_{cat}/K_M with rat arginase I; deletion of the α-carboxylate to yield agmatine results in an 11-fold increased K_M value and 54000-fold diminished catalytic activity. Comparable trends are observed for amino acid inhibitors of arginase; e.g., deletion of the carboxylate group of 2(*S*)-amino-6-boronohexanoic acid (ABH)[1] (*27*) to yield descarboxy-ABH results in an 1800-fold loss of inhibitory activity against rat arginase I (*28*).

[†] This work was supported by National Institutes of Health Grants GM67788 (D.E.A.) and GM49758 (D.W.C.) and by a Senior Investigator Award to D.W.C. from the Sandler Program for Asthma Research.

[‡] The atomic coordinates of unliganded T135A rat arginase I, the T135A rat arginase I−BEC complex, unliganded N130A rat arginase I, the D183N human arginase I−ABH complex, and the D183A human arginase I−ABH complex have been deposited in the Protein Data Bank (www.rcsb.org) with accession codes 3E8Q, 3E9B, 3E8Z, 3E6V, and 3E6K, respectively.

* To whom correspondence should be addressed. D.W.C.: tel, 215-898-5714; fax, 215-573-2201; e-mail, chris@sas.upenn.edu. D.E.A.: tel, 989-774-3981; fax, 989-774-3883; e-mail, ash1de@cmich.edu.

[§] University of Pennsylvania.

[||] Central Michigan University.

[⊥] Current address: Department of Biochemistry, Temple University School of Medicine, Philadelphia, PA 19140.

[1] Abbreviations: Bicine, *N*,*N*-bis(2-hydroxyethyl)glycine; CHES, 2-(*N*-cyclohexylamino)ethanesulfonic acid; HEPES, *N*-(2-hydroxyethyl)piperazine-*N*′-2-ethanesulfonic acid; PEG, polyethylene glycol; ABH, 2(*S*)-amino-6-boronohexanoic acid; BEC, *S*-(2-boronoethyl)-L-cysteine.

10.1021/bi801911v CCC: $40.75
Published on Web 12/18/2008

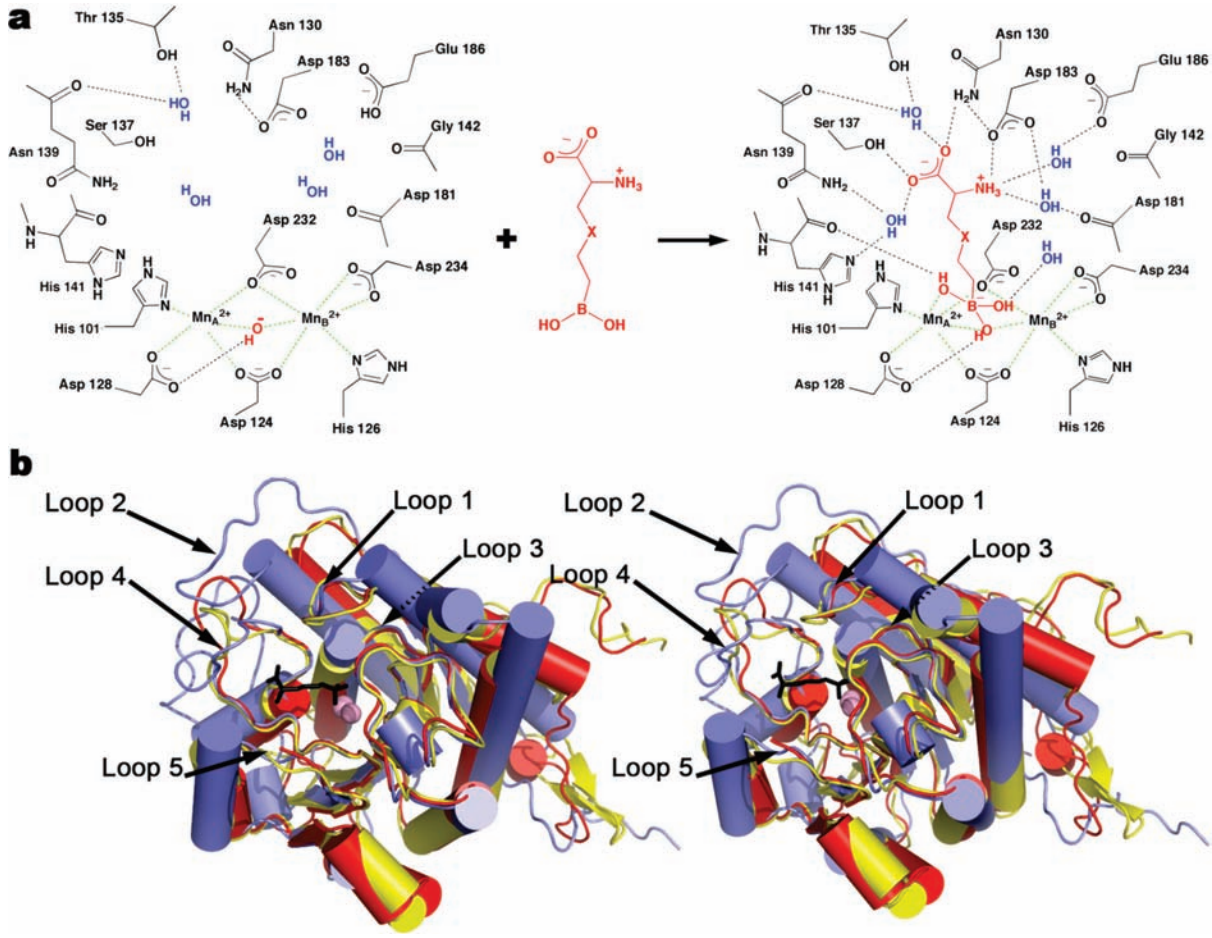

FIGURE 1: (a) Arginase I complexation with the substrate analogues *S*-(2-boronoethyl)-L-cysteine (BEC, X = S) or 2(*S*)-amino-6-boronohexanoic acid (ABH, X = CH_2) illustrates the constellation of hydrogen bond interactions with the α-amino and α-carboxylate groups responsible for molecular recognition of the amino acid moiety (*13*, *30*). These interactions are similarly conserved in the crystal structure of inactivated *B. caldovelox* arginase complexed with L-arginine (*29*). Residue numbers correspond to those of rat and human arginase I. (b) Stereoview of a least-squares superposition of human arginase I complexed with ABH (protein is in blue and ABH is in black; PDB accession code 2AEB) (*30*), agmatinase (in yellow; PDB accession code 1WOG) (*31*), and proclavaminic acid amidinohydrolase (in red; PDB accession code 1GQ6) (*32*). These enzymes share a common fold but exhibit significant variations in specificity loops 1, 2, 4, and 5. For reference, loop 3 is also indicated, but this loop does not flank the mouth of the active site. Active site Mn^{2+} ions are shown as purple spheres.

Thus, intact α-amino and α-carboxylate groups are the hallmarks of specificity for arginase substrates and inhibitors.

The specificity determinants of amino acid recognition by arginase were first illuminated by the X-ray crystal structures of the rat arginase I−ABH complex (*13*) and the complex between *Bacillus caldovelox* arginase inactivated by metal depletion and L-arginine (*29*). Both structures revealed an identical constellation of direct and water-mediated hydrogen bond interactions between conserved active site residues and the α-amino and α-carboxylate groups of the bound amino acid. More recently, the precise geometries of these interactions were confirmed in the crystal structures of human arginase I complexed with ABH and the related inhibitor S-(2-boronoethyl)-L-cysteine (BEC) (*30*).[2] Comparisons of the rat, human, and bacterial arginase structures reveal a conserved strategy for amino acid recognition and affinity in which α-substituents engage in the maximal number of hydrogen bond interactions; i.e., each oxygen of the α-carboxylate accepts two hydrogen bonds, and the α-amino group donates three hydrogen bonds (Figure 1a). Interestingly, the majority of enzyme−amino acid hydrogen bond interactions (four out of seven) accounting for such stringent substrate specificity are mediated by intervening water molecules.

The molecular recognition of the amino acid moiety of an arginase substrate or inhibitor is governed primarily by residues in two distinct loop segments: the α-carboxylate group engages in direct or water-mediated hydrogen bonds with N130, T135, S137, N139, and H141 in the loop connecting β-strand 4 and α-helix D (designated loop 4), and the α-amino group engages in direct or water-mediated hydrogen bonds with the backbone carbonyl of D181 and the carboxylate side chains of D183 and E186 in the loop connecting β-strand 5 and α-helix E (designated loop 5) (Figure 1b). It is notable that these loops, along with the loops connecting β-strand 1 and α-helix A1 (designated loop 1), and β-strand 2 and α-helix B (designated loop 2), exhibit significant structural variation when the arginase structure is compared with the structures of the related binuclear

[2] ABH and BEC are substrate analogues that contain a trigonal planar boronic acid moiety isosteric with the trigonal planar guanidinium moiety of L-arginine. Upon binding to the arginase active site, the trigonal planar boronic acid moiety of each inhibitor undergoes nucleophilic attack to yield a tetrahedral boronate anion that mimics the tetrahedral intermediate and its flanking transition states in the arginase reaction.

manganese metalloenzymes agmatinase (*31*) and proclavaminic acid amidinohydrolase (*32*) (Figure 1b). These enzymes hydrolyze guanidinium substrates that do not contain an intact amino acid moiety but otherwise resemble L-arginine. Thus, an emerging picture of substrate specificity in the active sites of arginase-like enzymes may be that the evolution of substrate recognition is governed in large part by mutations in loops 1, 2, 4, and 5, accordingly designated "specificity loops", that flank the mouth of the active site.

Here, we report studies of residues N130 and T135 in specificity loop 4 and D183 in specificity loop 5. These residues engage in direct or water-mediated hydrogen bond interactions with the α-amino and α-carboxylate groups of the amino acid substrate or inhibitors (Figure 1a). X-ray crystal structures of site-specific mutants of rat and human arginase I are correlated with measurements of enzyme activity and inhibitor binding to confirm that these residues play critical roles in amino acid recognition. However, mutation of these residues generally does not seriously impact catalytic activity. These results suggest that the evolution of altered substrate specificity is potentially facile and can proceed without significantly compromising the chemistry of guanidinium hydrolysis.

MATERIALS AND METHODS

Site-Directed Mutagenesis. Site-specific mutants of rat and human arginase I were prepared using the Stratagene QuikChange protocol. Nucleotide primers were purchased from Integrated DNA Technologies (Coralville, IA), and DNA sequencing was provided by the University of Pennsylvania DNA Sequencing Facility. Restriction enzymes were purchased from New England Biolabs. In rat arginase I, T135 was substituted to alanine or serine by replacing the appropriate codon (T135A, ACC → GCT; T135S, ACC → TCC) using wild-type cDNA as a template. Similarly, N130 was substituted to alanine, phenylalanine, or tyrosine in similar fashion (N130A, AAC → GCT; N130F, AAC → TTC; N130Y, AAC → TAC). In human arginase I, D183 was substituted to asparagine or alanine by replacing the appropriate codon (D183N, GAU → AAU; D183A, GAU → GCU) using wild-type cDNA as a template. All mutations were verified by nucleotide sequencing of the plasmid DNA. Rat arginase I mutants were overexpressed and purified from *Escherichia coli* BL21(DE3) cells using a pET29b expression vector (Novagen) as previously described (*33*), and human arginase I mutants were overexpressed and purified from *E. coli* BL21(DE3) cells using a pBS(KS) vector as previously described (*30, 34*). All mutant enzymes were homogeneous (>95% purity) as judged by SDS−PAGE under reducing conditions.

Enzyme Activity and Binding Assays. The catalytic activities of rat and human arginase I mutants were measured at room temperature using the fixed-point radioactive assay measuring [^{14}C]urea production developed by Rüegg and Russell (*35*) modified as described by Cavalli and colleagues (*33*). Briefly, all assays were performed in a reaction mixture of 100 mM CHES (pH 9.0), 100 μM $MnCl_2$, and approximately 0.05 μCi of L-[*guanido*-^{14}C]arginine (purchased from either NEN/PerkinElmer (specific activity = 2.5 GBq mmol^{-1}) or American Radiolabeled Chemicals, Inc. (specific activity = 1.95 GBq mmol^{-1})), with 1.0−20.0 mM unlabeled L-arginine. The reaction was allowed to proceed for 15 min following addition of mutant enzyme to the reaction mixture. Reactions were quenched with 0.25 mM acetic acid (pH 4.5), 7 M urea, and a 1:1 (v/v) slurry of Dowex W-X8 in water. Each reaction mixture was vortexed immediately after quenching and centrifuged at 6000 rpm for 10 min. A 200 μL volume of supernatant was removed, and 3 mL of scintillation liquid (EcoScint) was added for quantitation of [^{14}C]urea production using a Beckman scintillation counter (model LS 6000 SC). Control experiments showed that the assay was linear over the indicated time periods and that less than 10% of the substrate was consumed. Data were analyzed by double reciprocal plots of initial velocity measurements.

Scheme 1

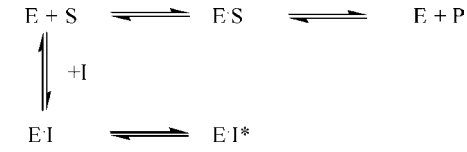

Slow onset inhibition of wild-type and T135S rat arginase I by BEC was analyzed by the addition of enzyme to the standard assay mixture in the presence of varying concentrations of BEC. Aliquots were removed at indicated times, and the [^{14}C]urea was analyzed as described above. Slow release kinetics were analyzed in similar manner except that enzyme preparations were equilibrated in a buffer solution containing 30 μM BEC for 15 min at room temperature prior to 100-fold dilution into a 1 mL reaction mixture containing 25 mM L-arginine and 0.05 μCi of L-[*guanido*-^{14}C]arginine. Progress curves for the arginase-catalyzed production of urea in the presence of BEC were fit by nonlinear least-squares analysis to the integrated expression in eq 1, where P = amount of urea formed (cpm), v_0 = initial rate of urea formation, v_s = steady-state rate of urea formation, and k_{obs} = apparent first-order rate constant for the equilibrium between E·I and E·I* (Scheme 1).

$$P = v_s(t) + (v_0 - v_s)(1 - e^{-k_{obs}(t)})/k_{obs} \quad (1)$$

Within the limitations of the assay, the initial velocities (v_0) appeared to be independent of inhibitor concentration, suggesting that the dissociation constant for the E·I complex was larger than the range of inhibitor concentrations used to generate the progress curves. Due to these limitations, the steady-state intermediate E·I was not observed, and therefore the binding of the inhibitor to arginase was approximated as a single-step process, E + I ⇌ E·I*, with $K_i = k_{off}/k_{on}$. The association rate constant, k_{on}, was estimated from a plot of k_{obs} (determined from an analysis of the progress curves using eq 1 above) versus inhibitor concentration, $k_{obs} = k_{off} + k_{on}[I]/(1 + [S]/K_m)$, for which the dissociation rate constant, k_{off}, was determined by monitoring the return of activity from the enzyme−inhibitor complex. A similar approach was utilized for the analysis of slow-binding inhibition of human arginase II by ABH and BEC (*36*).

The binding of ABH to D183N and D183A human arginase I mutants was assayed by isothermal titration calorimetry at 21 °C using a procedure identical to that described for determining the binding affinity of ABH to wild-type human arginase I (*30*). Briefly, enzyme was dialyzed against 50 mM bicine (pH 8.5) and 0.1 mM $MnCl_2$

Table 1: Data Collection and Refinement Statistics

	T135A rat arginase I (unliganded)	T135A rat arginase I−BEC complex	N130A rat arginase I (unliganded)	D183N human arginase I−ABH complex	D183A human arginase I−ABH complex
Data Collection					
resolution (Å)	50.0−2.90	50.0−2.15	60.4−2.00	30.0−1.72	50.0−2.10
total/unique reflections	53824/18754	145091/46355	144174/53201	147627/66499	89737/36884
R_{merge}[a,b]	0.136 (0.33)	0.107 (0.356)	0.077 (0.26)	0.058 (0.40)	0.067 (0.40)
completeness (%)[b]	96.3 (90.5)	98.8 (91.2)	91.8 (66.1)	97.0 (96.7)	98.6 (99.3)
$I/\sigma(I)$[b]	9.3 (2.7)	10.2 (2.1)	12.3 (3.0)	17.5 (2.0)	11.6 (2.0)
multiplicity[b]	2.9 (2.7)	3.1 (2.4)	2.7 (1.9)	2.2 (2.1)	2.4 (2.3)
Refinement					
reflections used in refinement/test set	17865/864	44988/4521	53196/2686	58910/2597	34893/1199
R/R_{free}[c]	0.263/0.296	0.216/0.274	0.241/0.282	0.219/0.232	0.164/0.245
protein atoms[d]	7026	7026	7026	4778	4670
water molecules[d]	46	339	275	368	141
Mn^{2+} ions[d]	6	6	6	4	4
BEC/ABH molecules[d]		3		2	2
rms Deviations					
bond lengths (Å)	0.008	0.006	0.005	0.006	0.007
bond angles (deg)	1.4	1.4	1.2	1.4	1.5
dihedral angles (deg)	23.0	22.8	20.5	22.9	23.3
improper dihedral angles (deg)	0.9	1.0	0.8	0.9	0.9

[a] $R_{merge} = \sum|I - \langle I\rangle|/\sum I$, where I is the observed intensity and $\langle I\rangle$ is the average intensity calculated for replicate data. [b] Number in parentheses refers to the outer 0.1 Å shell of data. [c] Crystallographic R-factor, $R = \sum(||F_o| - |F_c||)/\sum|F_o|$ for reflections contained in the working set. $R_{free} = \sum(||F_o| - |F_c||)/\sum|F_o|$ for reflections contained in the test set excluded from refinement. $|F_o|$ and $|F_c|$ are the observed and calculated structure factor amplitudes, respectively. [d] Per asymmetric unit.

at room temperature. The calorimeter cell contained ~60 μM enzyme, and the syringe contained 1.0 mM ABH. A series of 36 injections of 8 μL each were performed at 3 min intervals (two initial 2 μL injections were made but excluded from data analysis). The reaction mixture was continuously stirred. After each injection, the heat change was measured and converted to the corresponding enthalpy value. Data were fit to a single binding site model using Origin (v.2.9, Microcal, Inc.).

Crystallography. The T135A rat arginase I−BEC complex and unliganded N130A rat arginase I were crystallized by the hanging drop vapor diffusion method at 4 °C. Typically, drops containing 3 μL of protein solution [5 mg/mL protein, 50 mM bicine (pH 8.5), 2 mM BEC, 2 mM $MnCl_2$] and 3 μL of precipitant solution [0.1 M CHES (pH 9.5), 20% PEG 3350, 0.2 M NaCl] were equilibrated over a 1 mL reservoir of precipitant solution. Crystals of unliganded T135A rat arginase I were prepared in a similar fashion using a slightly different precipitant solution [0.1 M CHES (pH 9.5), 20% PEG 8000] and grew in 3 weeks. Crystals of unliganded T135A rat arginase I and the T135A rat arginase I−BEC complex were cryoprotected in the same precipitant solution augmented with 25% (w/v) sucrose, and crystals of unliganded N130A rat arginase I were cryoprotected in a precipitant solution augmented with 25% (w/v) glycerol. Crystals of T135A and N130A mutants were nearly isomorphous with those of wild-type rat arginase I (*37*).

The D183A and D183N mutants of human arginase I complexed with ABH were crystallized by the sitting drop vapor diffusion method at 21 °C. Typically, drops containing 4.0 μL of enzyme solution [3.5 mg/mL protein, 50.0 mM bicine (pH 8.5), 0.1 mM $MnCl_2$, 1.4 mM ABH] and 2.5 μL of precipitant solution [0.1 M HEPES (pH 7.0), 12−25% (w/v) Jeffamine ED-2001] were equilibrated against a 1 mL reservoir of precipitant solution. Crystals grew in 2 weeks and were nearly isomorphous with those of wild-type human arginase I (*30*). Crystals were subsequently soaked in a precipitant solution augmented with 10 mM ABH for 3 days and then cryoprotected in the same precipitant solution augmented with Jeffamine ED-2001 to a final concentration of 32% (w/v).

Diffraction data measured from crystals of rat and human arginase I mutants were collected at the Cornell High Energy Synchrotron Source (CHESS) on beamlines A1 or F2 or at the Brookhaven National Laboratory on beamline X12B. Intensity data integration and reduction were performed using MOSFLM (*38*) or the HKL suite of programs (*39*). Data reduction statistics are recorded in Table 1.

For crystal structure determinations of rat arginase I mutants, initial phasing was achieved by molecular replacement with AMoRe (*40*) using the structure of the native arginase trimer (PDB accession code 1RLA, less water molecules (*37*)) as a search probe for rotation and translation functions. Noncrystallographic symmetry constraints were employed in each refinement. Iterative rounds of refinement and model adjustment were performed using CNS and O, respectively (*41, 42*). Individual B-factors were refined, and a bulk solvent correction was applied. The atomic coordinates of BEC were included in the model during the final stages of refinement of the T135A rat arginase I−BEC complex. The N-terminus (M1−P5) and the C-terminus (P314−K323) were disordered and were excluded from each final model. Refinement statistics are recorded in Table 1. The quality of each final model was assessed using PROCHECK (*43*). Figures were generated using Pymol (*44*).

For human arginase I mutants, diffraction intensities measured from D183N and D183A crystals exhibited symmetry consistent with the apparent space group $P6$ (unit cell parameters $a = b = 91.0$ Å, $c = 69.8$ Å). As with crystals of other human arginase I−inhibitor complexes (*30*), deviations from ideal Wilson statistics were observed with $\langle I^2\rangle/\langle I\rangle^2 = 1.5$, indicating perfect hemihedral twinning (*45*). The structures of the D183N human arginase I−ABH complex and the D183A human arginase I−ABH complex were solved by molecular replacement using the program Phaser (*46*) with chain A of the human arginase I−ABH complex (PDB accession code 2ZAV, less water molecules) (*30*) used as a search probe against twinned data. In order to calculate

electron density maps, structure factor amplitudes ($|F_o|$) derived from twinned data ($|I_o|$) were deconvoluted into structure factor amplitudes corresponding to twin domains A and B ($|F_{o/A}|$ and $|F_{o/B}|$, respectively) using the structure-based algorithm of Redinbo and Yeates (*47*) implemented in CNS (*41*).

Crystallographic refinements of the D183N human arginase I−ABH and D183A human arginase I−ABH complexes against twinned data were performed as previously described for the wild-type enzyme−inhibitor complex (*30*). In the later stages of refinement after the majority of water molecules were located, gradient omit maps clearly showed ABH bound to the active site of each monomer in the asymmetric unit of the D183N human arginase I−ABH complex. The bound ABH molecule was refined with full occupancy to an average *B*-factor of 17 Å^2, consistent with the average *B*-factor of 18 Å^2 calculated for all protein atoms. For the structure determination of the D183A human arginase I−ABH complex, the occupancy of the ABH molecule was refined with occupancy = 0.5 to an average *B*-factor of 24 Å^2, consistent with the average *B*-factor of 26 Å^2 calculated for the entire protein. Disordered segments were excluded from the final models (M1−S5 and N319−K322 in D183N human arginase I, and M1−S5 and P314−K322 in D183A human arginase I). Data reduction and refinement statistics are recorded in Table 1. The quality of each refined model was assessed using PROCHECK (*43*). Figures were generated using Pymol (*44*).

RESULTS

T135 Rat Arginase I Mutants. In mammalian arginase I complexes with amino acid inhibitors BEC and ABH (*13*, *14*, *30*), the γ-hydroxyl group of T135 donates a hydrogen bond to a water molecule that, in turn, donates hydrogen bonds to the α-carboxylate of the bound amino acid and the backbone carbonyl of N139 (Figure 1a). Substitution of T135 with alanine destroys hydrogen-bonding potential, whereas substitution with serine conserves hydrogen-bonding potential. Indeed, in arginase from *B. caldovelox*, a serine residue is found in the corresponding position and makes an identical hydrogen bond interaction with a water molecule that donates a hydrogen bond to the α-carboxylate groups of bound amino acids (*29*). Kinetic parameters for the T135A and T135S mutants of rat arginase I are compared with those of the wild-type enzyme in Table 2. Notably, for T135A rat arginase I, the value of K_M is increased 13-fold, whereas the value of k_{cat} is reduced only 26%, relative to values measured for the wild-type enzyme. In contrast, for T135S rat arginase I, in which the γ-hydroxyl group is conserved, K_M increases only 2.5-fold and k_{cat} is unchanged relative to values measured for the wild-type enzyme. We conclude that the γ-hydroxyl side chain at position 135 functions along with the backbone carbonyl of N139 to orient a water molecule to donate a hydrogen bond to the α-carboxylate of the substrate. Deletion of the γ-hydroxyl group in the T135A mutant perturbs this enzyme−water−substrate hydrogen bond interaction and resultantly weakens enzyme−substrate affinity ~10-fold. Even so, mutagenesis of T135 does not significantly affect the chemistry of catalysis as reflected by minimal or no changes in k_{cat}.

Table 2: Kinetic Constants for Arginase Mutants[a]

mutant	K_M (mM)	k_{cat} (s^{-1})	k_{cat}/K_M (M^{-1} s^{-1})	K_i or K_d[b]
Rat Arginase I				
wild type	1.0	350	3.5×10^5	BEC,[c,d] K_i = 400 nM
T135A	13	260	2.0×10^4	BEC, K_i = 4500 nM
T135S	2.5	350	1.4×10^5	BEC,[c] K_i = 125 nM
N130A	50	220	4.4×10^3	BEC, K_i = 13000 nM
N130F	19.3	4.8	2.5×10^2	nd[e]
N130Y	21.4	17	7.9×10^2	nd[e]
D183A	13.9	14.7	1.1×10^3	nd[e]
Human Arginase I				
wild type[f]	1.5	190	1.3×10^5	ABH, K_d = 5 nM
D183A	136	68	5.0×10^2	ABH, K_d = 7000 nM
D183N	40	167	4.2×10^3	ABH, K_d = 147 nM

[a] Experimental errors are generally ±10%. [b] Inhibitory K_i values determined by enzyme assays and thermodynamic K_d values determined by isothermal titration calorimetry as described in the Materials and Methods section. [c] Slow-binding kinetics observed; $K_i = k_{off}/k_{on}$ as described in the Materials and Methods section. [d] Reference *14*. [e] nd, not determined. [f] References *30* and *48*.

While it is important that the T135 enzyme−water−substrate/inhibitor hydrogen bond interaction contributes a factor of ~10 to substrate/inhibitor affinity, it is additionally important to note the contribution of T135 to inhibitor binding kinetics. Studies with wild-type rat arginase I demonstrate that BEC is a slow-binding inhibitor with K_i = 400 nM (*14*). However, progress curves for T135A rat arginase I-catalyzed production of urea in the presence of 30 μM BEC are linear with time (Figure 2a), indicating that BEC does not exhibit slow-binding behavior to this mutant; inhibitor release is similarly rapid (Figure 2a, inset). Titration of the standard assay mixture with increasing concentrations of inhibitor yields K_i = 4500 nM. In contrast, progress curves shown in Figure 2b for the more conservative T135S mutant in the presence of BEC are decidedly nonlinear and indicative of slow-binding behavior. Replots of k_{obs} as a function of [BEC] yield $k_{on} = 1.24 \times 10^4$ M^{-1} s^{-1}. The slow release of BEC from the T135S mutant is shown in Figure 2b, inset, and the best fit of the release data yields $k_{off} = 1.55 \times 10^{-3}$ s^{-1}. Accordingly, $k_{off}/k_{on} = K_i$ = 125 nM.

X-ray crystal structure determinations of T135A rat arginase I in the presence and absence of BEC and comparisons with the structure of the wild-type enzyme complexed with BEC confirm the loss of this key enzyme−water−inhibitor hydrogen bond interaction. The T135A mutation does not affect the overall fold or the general active site structure of T135A rat arginase I, and the rms deviation of 312 Cα atoms with the unliganded wild-type enzyme is 0.32 Å. The structure of T135A rat arginase I complexed with BEC (Figure 3a) is nearly identical to that of the inhibitor complex with the wild-type enzyme (*14*) (rms deviation of 308 Cα atoms = 0.41 Å). However, hydrogen bond interactions are perturbed in the vicinity of the T135A mutation. In the wild-type arginase I−BEC complex, the hydroxyl group of T135 donates a hydrogen bond to a water molecule (no. 627 in monomer A and no. 644 in monomer B), and this water molecule in turn donates hydrogen bonds to the α-carboxylate group of BEC and the backbone carbonyl oxygen of N139. Of course, the A135 side chain cannot donate a hydrogen bond to the corresponding water molecule which remains bound in the T135A rat arginase I−BEC complex. However, this water molecule moves ~0.5 Å as a consequence of the T135A mutation. A superposition

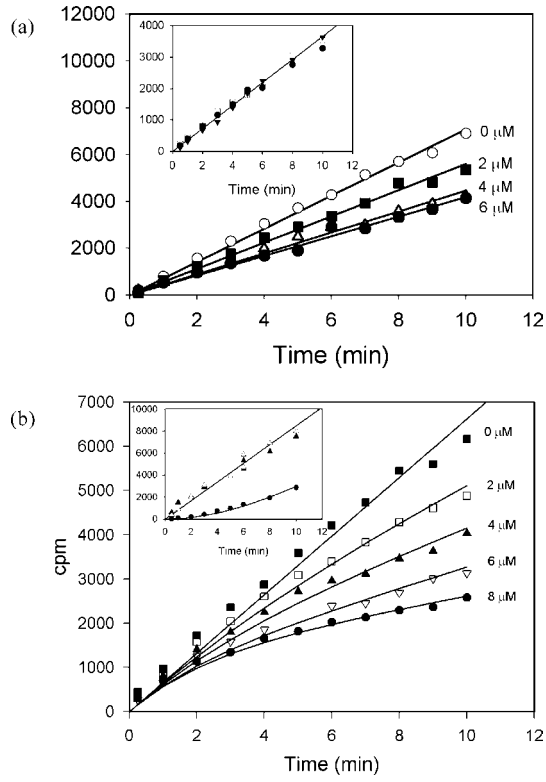

FIGURE 2: (a) Linear progress curves for BEC binding to T135A rat arginase do not reflect slow-binding inhibition kinetics. The enzyme was assayed as described in Materials and Methods at the indicated concentrations of BEC. Inset: Release of BEC from its complex with T135A rat arginase I. The straight line represents a control assay performed in the absence of BEC (□), an assay carried out in the presence of 0.3 μM BEC (●), and an assay carried out after 100-fold dilution of a preformed T135A rat arginase−BEC complex to give a final concentration of 0.3 μM BEC (▼). (b) Slow-binding inhibition of T135S rat arginase I by BEC. Progress curves were generated as described in Materials and Methods at the indicated concentrations of BEC. The curves represent the best fits of the data to eq 1 outlined in Materials and Methods. Inset: Release of BEC from its complex with T135S rat arginase I. The straight line represents a control assay performed in the absence of BEC (▲) and an assay carried out in the presence of 0.3 μM BEC (Δ). The curve represents the regain of activity following a 100-fold dilution of the preformed T135S−BEC complex to give a final concentration of 0.3 μM BEC (●). The estimated uncertainties in velocity measurements are ±10%.

of wild-type and T135A arginases I complexed with BEC is found in Figure 3b.

N130 Rat Arginase I Mutants. In mammalian arginase I complexes with amino acid inhibitors BEC and ABH (*13*, *14*, *30*), and in the bacterial arginase complex with L-arginine (*29*), the carboxamide NH_2 group of N130 donates hydrogen bonds to the α-carboxylate of the bound amino acid and the carboxylate group of D183 (Figure 1a). Kinetic parameters for the N130A, N130F, and N130Y mutants are compared with those of the wild-type enzyme in Table 2. Notably, for N130A rat arginase I, the value of K_M is increased 50-fold, whereas the value of k_{cat} is reduced only 37%, relative to values measured for the wild-type enzyme. Deletion of the α-carboxylate−N130 hydrogen bond by the N130A substitution significantly weakens enzyme−substrate affinity, as reflected by the significantly increased K_M value, but it does not significantly perturb the chemistry of catalysis, as reflected by only a modest decrease in k_{cat}. In contrast, the substitution of N130 with the bulky aromatic side chains of phenylalanine or tyrosine not only results in ∼20-fold increases in K_M, but these substitutions compromise the chemistry of catalysis as reflected by ∼80-fold or ∼20-fold reductions in k_{cat}, respectively. The bulky aromatic side chains presumably perturb substrate binding sufficiently to disrupt interactions required for catalysis elsewhere in the active site.

It is interesting to compare these results with those reported in previous studies of the more conservative N130D and N130Q mutants of human arginase I (*48*). Presuming that the D130 side chain can function in the protonated form as a carboxylic acid, both D130 and Q130 could preserve a hydrogen bond interaction with the α-carboxylate of the substrate. Accordingly, the N130D and N130Q substitutions increase K_M values more modestly, by 9-fold and 2-fold, respectively, with only modest effects on k_{cat}.

As observed for T135A rat arginase I, progress curves for N130A rat arginase I-catalyzed production of urea in the presence of 30 μM BEC are linear with time, indicating that, for this arginase mutant, BEC is no longer a slow-binding inhibitor, and inhibitor release is similarly rapid (data not shown). Titration of the standard assay mixture with increasing concentrations of inhibitor yields K_i = 13000 nM, indicating ∼30-fold diminished enzyme−inhibitor affinity. Thus, deletion of the N130 carboxamide significantly weakens enzyme−inhibitor affinity by deleting the hydrogen bond between the enzyme and the α-carboxylate of the amino acid inhibitor. We conclude that the hydrogen bond between the carboxamide side chain of N130 and the α-carboxylate of the substrate or inhibitor contributes a factor of ∼20−50 to affinity.

Although we were unsuccessful in preparing crystals of N130 rat arginase I mutants complexed with inhibitors, we were successful in determining the X-ray crystal structure of unliganded N130A rat arginase I. The N130A substitution does not affect the overall structure of the enzyme or the active site architecture, and the rms deviation of 288 Cα atoms is 0.23 Å between wild-type rat arginase I and N130A rat arginase I. Thus, the loss of substrate and inhibitor affinity resulting from the N130A mutation is due solely to the loss of hydrogen bond interactions with the side chain of N130 rather than an unanticipated conformational change in the active site. Surprisingly, even though BEC binds reasonably tightly to N130A rat arginase I and crystals of this mutant were grown in the presence of 2 mM BEC, the inhibitor is not bound in the active site. Instead, the characteristic metal-bridging solvent molecule of the unliganded enzyme (*37*, *49*) remains bound in this mutant (Figure 4).

D183 Rat and Human Arginase I Mutants. In mammalian arginase I complexes with amino acid inhibitors BEC and ABH (*13*, *14*, *30*), and in the bacterial arginase complex with L-arginine (*29*), the carboxylate group of D183 accepts hydrogen bonds from the α-amino group of the bound amino acid and also the carboxamide group of N130 (Figure 1a). In order to compare rat and human arginase I enzymes, we have selected the D183A mutant for parallel enzyme assays. For X-ray crystallographic purposes, human arginase I is more reliable in yielding higher quality crystals, so our studies of this mutant serve as a useful opportunity for a side-by-side comparison.

The kinetic parameters of rat and human wild-type enzymes and D183A mutants of the rat and human enzymes

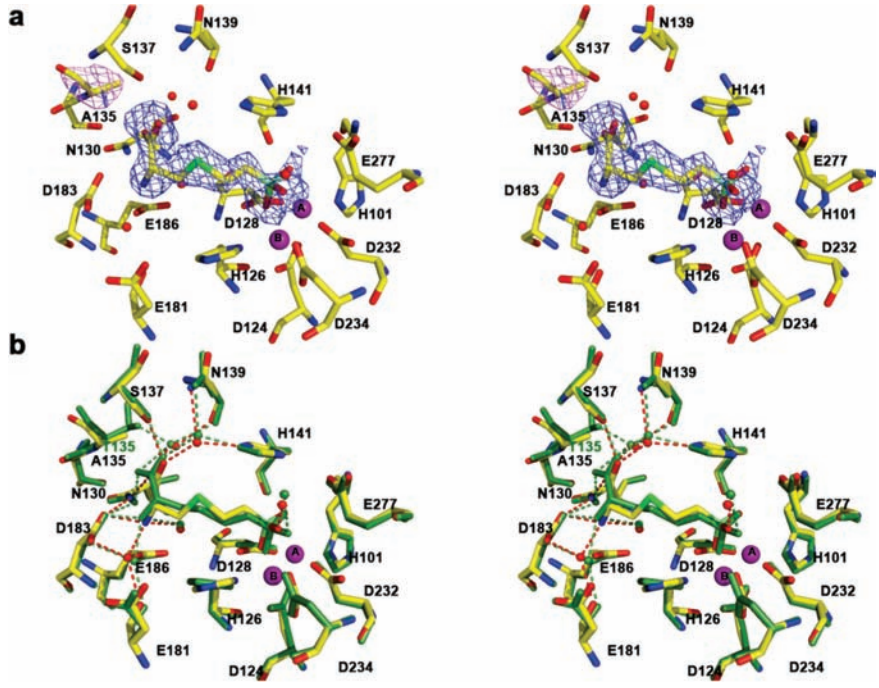

FIGURE 3: (a) Stereoview of simulated annealing omit electron density maps of the T135A arginase I−BEC complex (monomer A, contoured at 2.8σ) for which the atoms of BEC or A135 were omitted from the structure factor calculation. Active site Mn^{2+} ions and water molecules are shown as purple and red spheres, respectively. (b) Stereoview of a superposition of the wild-type (green) and T135A (color-coded as in (a)) rat arginase I−BEC complexes. Selected hydrogen bond interactions are indicated by dashed lines.

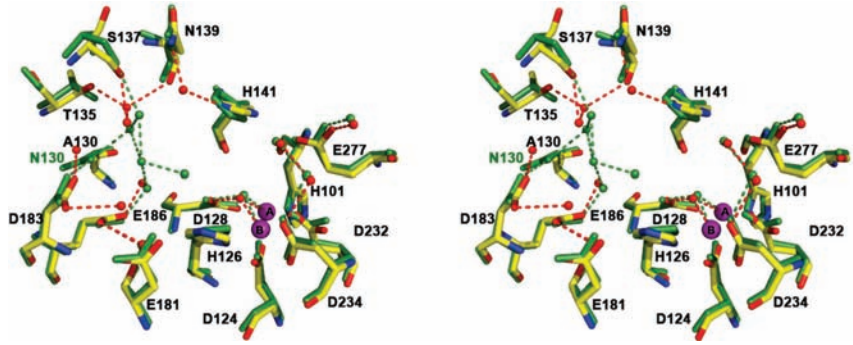

FIGURE 4: Stereoview of a superposition of the wild-type (green) and N130A (yellow) rat arginase I structures (monomers A). Active site Mn^{2+} ions and water molecules are shown as purple and red spheres, respectively. Selected hydrogen bond interactions are indicated by dashed lines.

exhibit moderately similar trends (Table 2). For D183A rat arginase I, the value of K_M is increased 14-fold, whereas the value of k_{cat} is reduced 24-fold, relative to values measured for the wild-type enzyme. For D183A human arginase I, the value of K_M is increased 91-fold, whereas the value of k_{cat} is reduced only ~3-fold, relative to values measured for the wild-type enzyme. Therefore, deletion of the substrate α-amino−D183 hydrogen bond by the D183A substitution significantly weakens enzyme−substrate affinity, as reflected by the significantly increased K_M values, and also perturbs the chemistry of catalysis, as reflected by decreased k_{cat} values. In comparison, the D183N substitution results in comparatively modest changes: K_M is increased 27-fold and k_{cat} is reduced by only 12% relative to values measured for the wild-type enzyme. That substrate affinity is more significantly affected in the D183A mutant compared with the D183N mutant likely reflects the fact that A183 cannot engage in hydrogen bond interactions, whereas the Oδ atom of N183 is isosteric with the Oδ1 atom of D183 and can therefore accept a hydrogen bond from the substrate α-amino group. Affinity may be somewhat weaker, however, due to the electrostatic consequences of substituting a charge−charge hydrogen bond with a slightly weaker (*50*) dipole−charge hydrogen bond.

With regard to inhibitor binding, calorimetric measurements of the ABH dissociation constant reveal that inhibitor binding affinity is weakened ~1400-fold in the D183A human arginase I−ABH complex relative to the complex with the wild-type enzyme, whereas inhibitor binding affinity is weakened 29-fold in the D183N human arginase I−ABH complex (Table 2). The trend of diminished inhibitor affinity to D183A and D183N enzymes generally mirrors the trend of diminished substrate affinity.

The X-ray crystal structures of D183N and D183A human arginase I mutants complexed with ABH reveal that the mutations do not affect the overall protein fold, nor do they perturb the general active site structure. The rms deviations of 313 Cα atoms between mutant and wild-type enzyme complexes with ABH are 0.22 and 0.35 Å, respectively. The binding mode of ABH in the active site of each mutant enzyme is essentially conserved with respect to its binding mode in the active site of the wild-type enzyme (*30*).

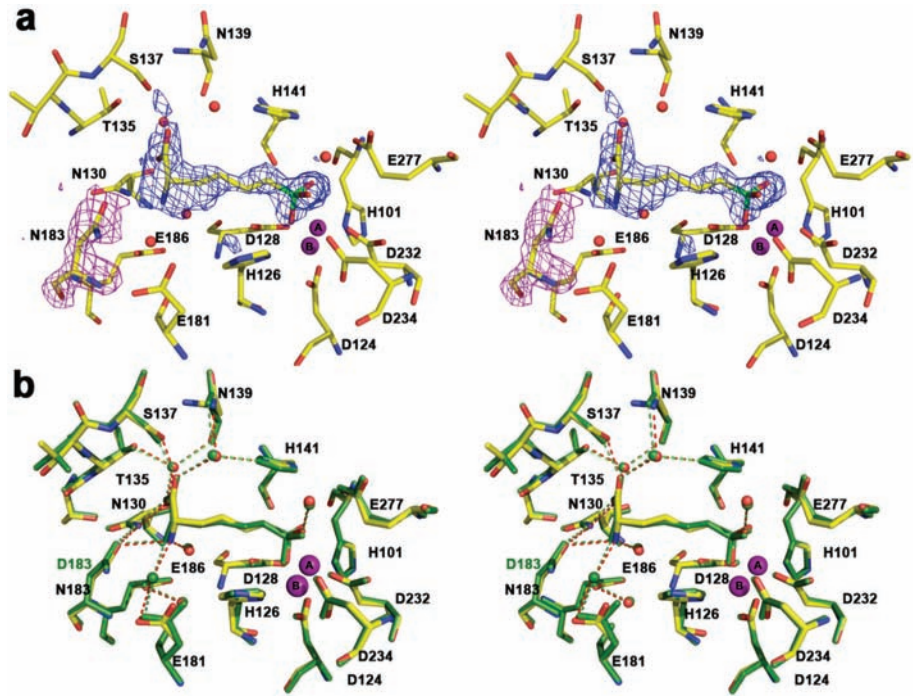

FIGURE 5: (a) Stereoview of simulated annealing omit electron density maps of the D183N human arginase I−ABH complex, contoured at 3.0σ (N183) and 2.5σ (ABH). Active site Mn^{2+} ions and water molecules are shown as purple and red spheres, respectively. (b) Stereoview of a superposition of the wild-type human arginase I−ABH complex (green) and the D183N human arginase I−ABH complex (color-coded as in (a)). The ABH−water hydrogen bond interactions are indicated by dashed lines.

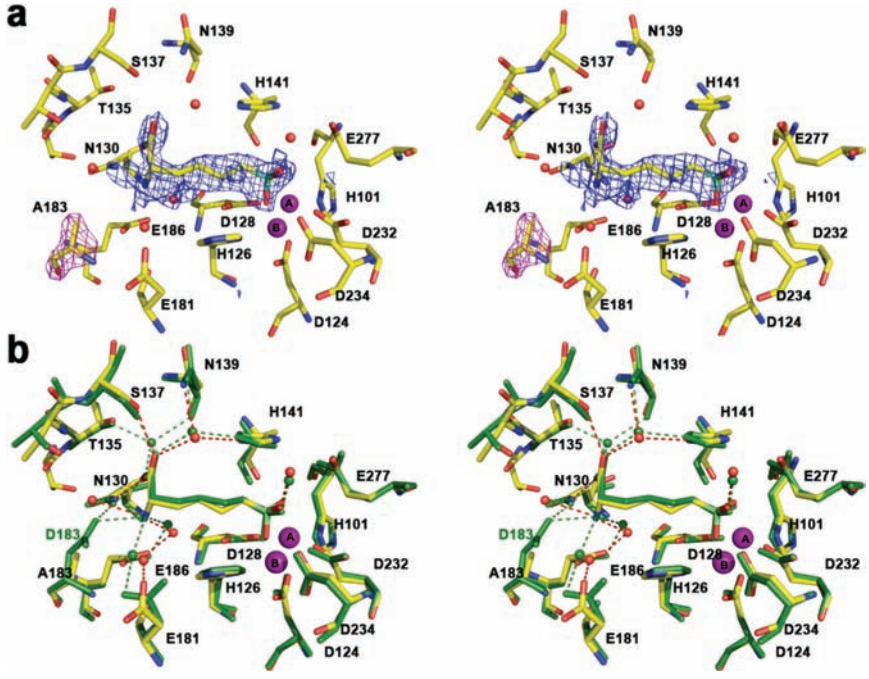

FIGURE 6: (a) Stereoview of simulated annealing omit electron density maps of the D183A human arginase I−ABH complex, contoured at 3.0σ (A183) and 2.5σ (ABH). Active site Mn^{2+} ions and water molecules are shown as purple and red spheres, respectively. (b) Stereoview of a superposition of the wild-type human arginase I−ABH complex (green) and the D183A human arginase I−ABH complex (color-coded as in (a)). The ABH−water hydrogen bond interactions are indicated by dashed lines.

The α-carboxylate and α-amino groups of ABH are anchored to the active site of the D183N human arginase I−ABH complex by three direct and four water-mediated hydrogen bonds, as observed in the wild-type human arginase I−ABH complex, except that the carboxamide C═O group of N183 is positioned to accept a hydrogen bond from the α-amino group of ABH (Figure 5). Thus, diminished inhibitor affinity resulting from the D183N substitution results solely from the altered electrostatics of the interaction with the α-amino group of the inhibitor. In contrast, the D183A substitution completely abolishes the hydrogen bond with the α-amino group of the inhibitor, resulting in 1400-fold diminished affinity as well as a diminished occupancy of 0.5 for inhibitor binding in the crystal structure (Figure 6). A water molecule resides in former location of the carboxylate side chain of D183 and accepts a hydrogen bond from the α-amino group of the inhibitor.

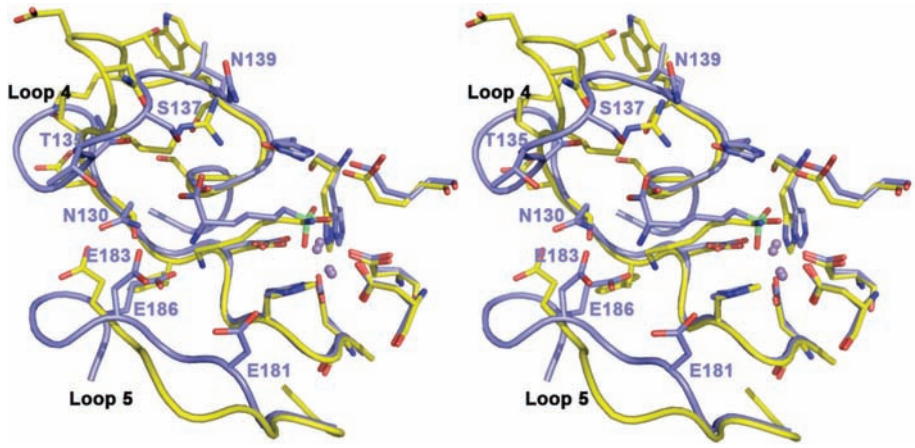

FIGURE 7: Stereoview of a superposition of the human arginase I−ABH complex (blue) (*30*) and the agmatinase−1,6-diaminohexane complex (yellow) (*31*) illustrates how structural differences in specificity loops 4 and 5, which flank the mouth of the active site, accommodate the binding of alternative ligands in binuclear manganese metalloenzymes sharing the same fold. The orientation is the same as that in Figure 1b but zoomed in on the active site.

DISCUSSION

Substrate and inhibitor binding in the active site of arginase requires an intact L-amino acid moiety, as first demonstrated by Reczkowski and Ash in the exploration of alternative guanidinium substrates (*26*). Here, we dissect the molecular basis of amino acid recognition in the arginase active site by perturbing direct and water-mediated hydrogen bonds hypothesized to be critical for enzyme−substrate and enzyme−inhibitor recognition. For binding to mutant enzymes, increased inhibitor K_d values generally correspond with increased substrate K_M values, in that the largest increases result from the perturbation of a direct charged hydrogen bond with D183, the next largest increases result from the perturbation of a direct hydrogen bond with N130, and the smallest increases result from the perturbation of a water-mediated hydrogen bond with T135. While it is important not to overinterpret these data, a general trend is discernible suggesting that the relative contribution of intermolecular interactions to amino acid affinity in the arginase active site is water-mediated hydrogen bond < direct hydrogen bond < direct charged hydrogen bond.

The α-carboxylate of the amino acid makes two direct and two water-mediated hydrogen bond interactions in the active site of arginase (Figure 1a). Perturbation of a water-mediated hydrogen bond interaction in the T135A mutant results in 13-fold diminished substrate affinity (as indicated by K_M) and 11-fold diminished inhibitor affinity; perturbation of a direct hydrogen bond interaction in the N130A mutant results in 50-fold diminished substrate affinity and 32-fold diminished inhibitor affinity (Table 2). Thus, the direct hydrogen bond interaction makes a more pronounced contribution to affinity than the water-mediated hydrogen bond interaction. It is instructive to compare these parameters with those measured between wild-type rat arginase I and the alternative substrate agmatine (*26*) and its boronic acid analogue descarboxy-ABH (*28*), both of which lack the α-carboxylate moiety: here, substrate affinity is diminished 11-fold and inhibitor affinity is diminished 30000-fold. Inhibitor affinity appears to be more sensitive than substrate affinity to the complete loss of all four hydrogen bond interactions with the α-carboxylate moiety of the amino acid. Perhaps this reflects the evolutionary potential of N130 and its associated loop 4 as a "hot spot" in the evolution of substrate specificity as noted by Carvajal (*48*), given that the arginase fold is shared by agmatinase (*31*). Intriguingly, Carvajal further reports that although N130D human arginase I exhibits 9-fold diminished substrate affinity with L-arginine, this mutation confers agmatinase activity with K_M and k_{cat} values of 1.4 mM and 3 s^{-1}, respectively (*48*). These values compare with K_M and k_{cat} values values of 1.5 mM and 140 s^{-1}, respectively, measured for wild-type agmatinase from *E. coli* (*51*).

Given that slow-binding inhibition of rat arginase I by BEC is measured for wild-type human arginase II (*36*), wild-type rat arginase I (*14*), and T135S rat arginase I (Figure 2b), and given that slow-binding inhibition by BEC or ABH is not observed for the T135A, N130A, or D183A mutants, we conclude that the observation of slow-binding inhibitory kinetics requires an intact constellation of residues that function in the stereospecific molecular recognition of the L-amino acid moiety. While it might be tempting to speculate that hydrogen bond interactions of the amino acid moiety with these residues are responsible for the slow-binding behavior observed for boronic acid inhibitor binding to wild-type or T135S rat arginase I, it is perhaps more likely that the unobserved slow-binding kinetics may simply be a consequence of weakened inhibitor binding. That is, the molecular basis of slow-binding kinetics itself need not necessarily be compromised by the deleted hydrogen bond interactions, but such kinetics may simply escape detection due to the higher K_i value for inhibitor binding to the mutant enzyme. Compromised molecular recognition of the amino acid moiety results in weaker affinity and a higher k_{off} value that can potentially mask an underlying slow-binding k_{on} value. Slow-binding kinetics observed for ABH and BEC binding to human arginase II are rooted in the interconversion of the side chain boronic acid moiety from its trigonal planar state to the tetrahedral boronate anion (*36*), and it is likely that the molecular basis of slow-binding kinetics observed for ABH and BEC to rat arginase I has a similar origin (*14*, *27*). Significantly, slow-binding behavior of peptide boronic acid inhibitors to serine proteases is similarly observed (*52*) and is attributed to rate-determining nucleophilic addition to the boronic acid moiety (*53*).

In addition to the crystal structure determination of agmatinase from *Deinococcus radiodurans* (*31*), the crystal structure of proclavaminic acid amidinohydrolase from *Streptomyces clavuligerus* has been recently reported (*32*). The overall amino acid sequence identities of these enzymes with rat/human arginase I are 37/39% and 29/30%, respectively. These enzymes share the arginase fold and also share strictly conserved residues important for metal binding (H101, D124, H126, D128, D232, and D234) and catalysis (D128, E277, and H141).[3] However, the amino acid sequences and structures of these enzymes are significantly divergent in loops 4 and 5 (Figure 1b), which contain the residues responsible for the molecular recognition of the amino acid moiety of substrate and inhibitors. Of the arginase residues that engage in direct or water-mediated hydrogen bonds with the α-carboxylate group of the substrate (N130, T135, S137, N139, and H141 in loop 4), only N130 and H141 are conserved in proclavaminic acid amidinohydrolase (*32*), perhaps because its guanidine substrate similarly contains an intact α-carboxylate group. None of these residues are conserved in agmatinase from *D. radiodurans*. It is also interesting to note that although proclavaminic acid amidinohydrolase does not accept L-arginine as a substrate (*54*), this enzyme catalyzes the hydrolysis of L-arginine derivatives (*55*) bearing acetylated α-amino groups (*32*). Of the arginase residue side chains that engage in direct or water-mediated hydrogen bonds with the α-amino group of the substrate (D183 and E186 in loop 5), only D183 is conserved in agmatinase from *D. radiodurans* (*32*), perhaps because its substrate similarly contains an intact α-amino group. Ligand binding to arginase and agmatinase is compared in Figure 7.

Parenthetically, we note that although the crystal structure of D-arginase from *Arthrobacter* sp. KUJ 8602 (also known as guanidinobutyrase) has not yet been determined, amino acid sequence alignments indicate 24−29% overall identity with arginase I enzymes from rat and human and arginase from *B. caldovelox*, and all residues required for metal binding and the chemistry of catalysis are strictly conserved (*56*). However, none of the residues required for the molecular recognition of an L-amino acid in specificity loops 4 and 5 are conserved. Thus, the evolution of catalytic specificity in the arginase fold includes not only guanidinium substrates with alternative structures but also the arginine substrate itself with opposite stereochemistry.

Thus, structural comparisons with agmatinase and proclavaminic acid amidinohydrolase suggest that the evolution of substrate recognition in the arginase fold is mediated by mutations in specificity loops 1, 2, 4, and 5 flanking the mouth of the active site (Figure 1b) so that diverse guanidinium substrates can be accommodated. To this end, it is intriguing to speculate that the significant number of water-mediated hydrogen bonds involved in the molecular recognition of the amino acid bound in the active site (Figure 1a) may somehow reflect enhanced potential for the evolution of molecular recognition: while a water-filled cleft provides ample opportunity for hydrogen bond interactions between enzyme and substrate, it also provides additional active site volume that is potentially adaptable to the binding of alternative substrates; amino acid mutations in loops defining this volume can easily reshape the active site contour in the evolution of substrate specificity. Future structural and functional studies with arginase I will potentially allow us to further explore and engineer biosynthetic diversity with alternative guanidinium substrates.

[3] H141 is conserved in agmatinase from *E. coli* and human, but the corresponding residue appears as asparagine in agmatinase from *D. radiodurans*. This is interesting in view of the significant residual catalytic activity observed in H141N rat arginase I (*33*).

ACKNOWLEDGMENT

We thank Professor Ronen Marmorstein for the use of his calorimeter for the isothermal titration calorimetry measurements.

REFERENCES

1. Ash, D. E., Cox, J. D., and Christianson, D. W. (2000) Arginase: a binuclear manganese metalloenzyme. *Met. Ions Biol. Syst. 37*, 407–428.
2. Morris, S. M., Jr. (2002) Regulation of enzymes of the urea cycle and arginine metabolism. *Annu. Rev. Nutr. 22*, 87–105.
3. Ash, D. E. (2004) Structure and function of arginases. *J. Nutr. 134*, 2760S–2764S.
4. Christianson, D. W. (2005) Arginase: structure, mechanism, and physiological role in male and female sexual arousal. *Acc. Chem. Res. 101*, 191–201.
5. Krebs, H. A., and Henseleit, K. (1932) Untersuchungen über die Harnstoffbildung im tierkorper. *Z. Physiol. Chem. 210*, 33–66.
6. Herzfeld, A., and Raper, S. M. (1976) The heterogeneity of arginases in rat tissues. *Biochem. J. 153*, 469–478.
7. Kossel, A., and Dakin, H. D. (1904) Über die arginase. *Z. Physiol. Chem. 41*, 321–331.
8. Morris, S. M., Jr. (2000) Regulation of arginine availability and its impact on NO synthesis, *Nitric Oxide. Biology and Pathobiology* (Ignarro, L. J., Ed.) pp 187−197, Academic Press, San Diego, CA.
9. Mori, M., and Gotoh, T. (2000) Relationship between arginase activity and nitric oxide production, *Nitric Oxide. Biology and Pathobiology* (Ignarro, L. J., Ed.) pp 199−208, Academic Press, San Diego, CA.
10. Morris, S. M., Jr. (2004) Enzymes of arginine metabolism. *J. Nutr. 134*, 2743S–2747S.
11. Tabor, C. W., and Tabor, H. (1984) Polyamines. *Annu. Rev. Biochem. 53*, 749–790.
12. Yip, M. C. M., and Knox, W. E. (1972) Function of arginase in lactating mammary gland. *Biochem. J. 127*, 893–899.
13. Cox, J. D., Kim, N. N., Traish, A. M., and Christianson, D. W. (1999) Arginase-boronic acid complex highlights a physiological role in erectile function. *Nat. Struct. Biol. 6*, 1043–1047.
14. Kim, N. N., Cox, J. D., Baggio, R. F., Emig, F. A., Mistry, S. K., Harper, S. L., Speicher, D. W., Morris, S. M., Ash, D. E., Traish, A., and Christianson, D. W. (2001) Probing erectile function: *S*-(2-boronoethyl)-L-cysteine binds to arginase as a transition state analogue and enhances smooth muscle relaxation in human penile corpus cavernosum. *Biochemistry 40*, 2678–2688.
15. Bivalacqua, T. J., Hellstrom, W. J., Kadowitz, P. J., and Champion, H. C. (2001) Increased expression of arginase II in human diabetic corpus cavernosum: in diabetic-associated erectile dysfunction. *Biochem. Biophys. Res. Commun. 283*, 923–927.
16. Kim, N. N., Christianson, D. W., and Traish, A. M. (2004) Role of arginase in the male and female sexual arousal response. *J. Nutr. 134*, 2873S–2879S.
17. Bivalacqua, T. J., Burnett, A. L., Hellstrom, W. J., and Champion, H. C. (2007) Overexpression of arginase in the aged mouse penis impairs erectile function and decreases eNOS activity: influence of in vivo gene therapy of anti-arginase. *Am. J. Physiol. Heart Circ. Physiol. 292*, H1340−H1351.
18. Zimmermann, N., King, N. E., Laporte, J., Yang, M., Mishra, A., Pope, S. M., Muntel, E. E., Witte, D. P., Pegg, A. A., Foster, P. S., Hamid, Q., and Rothenberg, M. E. (2003) Dissection of experimental asthma with DNA microarray analysis identifies arginase in asthma pathogenesis. *J. Clin. Invest. 111*, 1863–1874.
19. Meurs, H., McKay, S., Maarsingh, H., Hamer, M. A. M., Macic, L., Molendijk, N., and Zaagsma, J. (2002) Increased arginase activity underlies allergen-induced deficiency of cNOS-derived nitric oxide and airway hyperresponsiveness. *Br. J. Pharmacol. 136*, 391–398.

20. Meurs, H., Maarsingh, H., and Zaagsma, J. (2003) Arginase and asthma: novel insights into nitric oxide homeostasis and airway hyperresponsiveness. *Trends Pharmacol. Sci. 24*, 450–455.
21. Yang, M., Rangasamy, D., Matthaei, K. I., Frew, A. J., Zimmermann, N., Mahalingam, S., Webb, D. C., Tremethick, D. J., Thompson, P. J., Hogan, S. P., Rothenberg, M. E., Cowden, W. B., and Foster, P. S. (2006) Inhibition of arginase I activity by RNA interference attenuates IL-13-induced airways hyperresponsiveness. *J. Immunol. 177*, 5595–5603.
22. Berkowitz, D. E., White, R., Li, D., Minhas, K. M., Cernetich, A., Kim, S., Burke, S., Shoukas, A. A., Nyhan, D., Champion, H. C., and Hare, J. M. (2003) Arginase reciprocally regulates nitric oxide synthase activity and contributes to endothelial dysfunction in aging blood vessels. *Circulation 108*, 2000–2006.
23. Ming, X. F., Barandier, C., Viswabharan, H., Kwak, B. R., Mach, F., Mazzolai, L., Hayoz, D., Ruffieux, J., Rusconi, S., Montani, J. P., and Yang, Z. (2004) Thrombin stimulates human endothelial arginase enzymatic activity via RhoA/ROCK pathway: implications for atherosclerotic endothelial dysfunction. *Circulation 110*, 3708–3714.
24. Yang, Z., and Ming, X.-F. (2006) Endothelial arginase: a new target in atherosclerosis. *Curr. Hypertension Rep. 8*, 54–59.
25. Ryoo, S., Gupta, G., Benjo, A., Lim, H. K., Camara, A., Sikka, G., Lim, H. K., Sohi, J., Santhanam, L., Soucy, K., Tuday, E., Baraban, E., Ilies, M., Gerstenblith, G., Nyhan, D., Shoukas, A., Christianson, D. W., Alp, N. J., Champion, H. C., Huso, D., and Berkowitz, D. E. (2008) Endothelial arginase II: a novel target for the treatment of atherosclerosis. *Circ. Res. 102*, 923–932.
26. Reczkowski, R. S., and Ash, D. E. (1994) Rat liver arginase: kinetic mechanism, alternate substrates, and inhibitors. *Arch. Biochem. Biophys. 312*, 31–37.
27. Baggio, R., Elbaum, D., Kanyo, Z. F., Carroll, P. J., Cavalli, R. C., Ash, D. E., and Christianson, D. W. (1997) Inhibition of $Mn^{2+}{}_2$-arginase by borate leads to the design of a transition state analogue inhibitor, 2(*S*)-amino-6-boronohexanoic acid. *J. Am. Chem. Soc. 119*, 8107–8108.
28. Collet, S., Carreaux, F., Boucher, J.-L., Pethe, S., Lepoivre, M., Danion-Bougot, R., and Danion, D. (2000) Synthesis and evaluation of ω-borono-α-amino acids as active-site probes of arginase and nitric oxide synthases. *J. Chem. Soc., Perkin Trans. 1*, 177–182.
29. Bewley, M. C., Jeffrey, P. D., Patchett, M. L., Kanyo, Z. F., and Baker, E. N. (1999) Crystal structures of *Bacillus caldovelox* arginase in complex with substrate and inhibitors reveal new insights into activation, inhibition and catalysis in the arginase superfamily. *Structure 7*, 435–448.
30. Di Costanzo, L., Sabio, G., Mora, A., Rodriguez, P. C., Ochoa, A. C., Centeno, F., and Christianson, D. W. (2005) Crystal structure of human arginase I at 1.29 Å resolution and exploration of inhibition in the immune response. *Proc. Natl. Acad. Sci. U.S.A. 102*, 13058–13063.
31. Ahn, H. J., Kim, K. H., Lee, J., Ha, J.-Y., Lee, H. H., Kim, D., Yoon, H.-J., Kwon, A.-R., and Suh, S. W. (2004) Crystal structure of agmatinase reveals structural conservation and inhibition mechanism of the ureohydrolase superfamily. *J. Biol. Chem. 279*, 50505–50513.
32. Elkins, J. M., Clifton, I. J., Hernpández, H., Doan, L. X., Robinson, C. V., Schofield, C. J., and Hewitson, K. S. (2002) Oligomeric structure of proclavaminic acid amidino hydrolase: evolution of a hydrolytic enzyme in clavulanic acid biosynthesis. *Biochem. J. 366*, 423–434.
33. Cavalli, R. C., Burke, C. J., Kawamoto, S., Soprano, D. R., and Ash, D. E. (1994) Mutagenesis of rat liver arginase expressed in *Escherichia coli*: role of conserved histidines. *Biochemistry 33*, 10652–10657.
34. Mora, A., del Ara Rangel, M., Fuentes, J. M., Soler, G., and Centeno, F. (2000) *Biochim. Biophys. Acta 1476*, 181–190.
35. Rüegg, U. T., and Russell, A. S. (1980) A rapid and sensitive assay for arginase. *Anal. Biochem. 102*, 206–212.
36. Colleluori, D. M., and Ash, D. E. (2001) Classical and slow-binding inhibitors of human type II arginase. *Biochemistry 40*, 9356–9362.
37. Kanyo, Z. F., Scolnick, L. R., Ash, D. E., and Christianson, D. W. (1996) Structure of a unique binuclear manganese cluster in arginase. *Nature 383*, 554–557.
38. Leslie, A. G. W. (1990) Molecular data processing, in *Crystallographic Computing 5: from Chemistry to Biology* (Moras, D., Podjarny, A. D., and Thierry, J.-C., Eds.) pp 50−61, Oxford University Press, Oxford, U.K.
39. Otwinowski, Z., and Minor, W. (1997) Processing of X-ray diffraction data collected in oscillation mode. *Methods Enzymol. 276*, 307–326.
40. Navaza, J. (1994) AMoRe: an automated package for molecular replacement. *Acta Crystallogr. A50*, 157–163.
41. Brünger, A. T., Adams, P. D., Clore, G. M., DeLano, W. L., Gros, P., Grosse-Kunstleve, R. W., Jiang, J.-S., Kuszewski, J., Nilges, M., Pannu, N. S., Read, R. J., Rice, L. M., Simonson, T., and Warren, G. L. (1988) Crystallography and NMR system: a new software suite for macromolecular structure determination. *Acta Crystallogr. D54*, 905–921.
42. Jones, T. A., Zou, J.-Y., Cowan, S. W., and Kjeldgaard, M. (1991) Improved methods for building protein models in electron density maps and the location of errors in these models. *Acta Crystallogr. A47*, 110–119.
43. Laskowski, R. A., MacArthur, M. W., Moss, D. S., and Thornton, J. M. (1993) PROCHECK: a program to check the stereochemical quality of protein structures. *J. Appl. Crystallogr. 26*, 283–291.
44. DeLano, W. L. (2002) The PyMOL Molecular Graphics System, DeLano Scientific LLC, San Carlos, CA(http://www.pymol.org).
45. Yeates, T. O. (1997) Detecting and overcoming crystal twinning. *Methods Enzymol. 276*, 344–358.
46. Zwart, P. H., Afonine, P. V., Grosse-Kunstleve, R. W., Hung, L. W., Ioerger, T. R., McCoy, A. J., McKee, E., Moriarty, N. W., Read, R. J., Sacchettini, J. C., Sauter, N. K., Storoni, L. C., Terwilliger, T. C., and Adams, P. D. (2008) Automated structure solution with the PHENIX suite. *Methods Mol. Biol. 426*, 419–435.
47. Redinbo, M. R., and Yeates, T. O. (1993) Structure determination of plastocyanin from a specimen with a hemihedral twinning fraction of one-half. *Acta Crystallogr. D49*, 375–380.
48. Alarcón, R., Orellana, M. S., Neira, B., Uribe, E., Garcia, J. R., and Carvajal, N. (2006) Mutational analysis of substrate recognition by human arginase type I-agmatinase activity of the N130D variant. *FEBS J. 273*, 5625–5631.
49. Di Costanzo, L., Pique, M. E., and Christianson, D. W. (2007) Crystal structure of human arginase I complexed with thiosemicarbazide reveals an unusual thiocarbonyl μ-sulfide ligand in the binuclear manganese cluster. *J. Am. Chem. Soc. 129*, 6388–6389.
50. Burley, S. K., and Petsko, G. A. (1988) Weakly polar interactions in proteins. *Adv. Protein Chem. 39*, 125–189.
51. Carvajal, N., López, V., Salas, M., Uribe, E., Herrera, P., and Cerpa, J. (1999) Manganese is essential for catalytic activity of *Escherichia coli* agmatinase. *Biochem. Biophys. Res. Commun. 258*, 808–811.
52. Kettner, C. A., and Shenvi, A. B. (1984) Inhibition of the serine proteases leukocyte elastase, cathepsin G, and chymotrypsin by peptide boronic acids. *J. Biol. Chem. 259*, 15106–15114.
53. Nakatani, H., Uehara, Y., and Hiromi, K. (1975) Elementary processes in the interaction of serine protease with a possible transition state analogue. *J. Biochem. 78*, 611–616.
54. Elson, S. W., Baggaley, K. H., Davison, M., Fulston, M., Nicholson, N. H., Risbridger, G. D., and Tyler, J. W. (1993) The identification of three new biosynthetic intermediates and one further biosynthetic enzyme in the clavulanic acid pathway. *J. Chem. Soc., Chem. Commun.*, 1212–1214.
55. Baldwin, J. E., Lee, V., Lloyd, M. D., Schofield, C. J., Elson, S. W., and Baggaley, K. H. (1993) Substrate analogue studies on clavaminic acid synthase. *J. Chem. Soc., Chem. Commun.*, 1694–1696.
56. Arakawa, N., Igarashi, M., Kazuoka, T., Oikawa, T., and Soda, K. (2003) D-Arginase of *Arthrobacter* sp. KUJ 8602: characterization and its identity with Zn^{2+}-guanidinobutyrase. *J. Biochem. 133*, 33–42.

BI801911V